電気学会論文誌●（●●●●●●●部門誌）
IEEJ Transactions on ●●●●●●●●●●●●●●●
Vol.●● No.● pp.●-● DOI: ●.●●/ieejeiss.●●.●

Paper

Parallel Connected Multiple Motor Drive System Using Small Auxiliary Inverter for Permanent Magnet Synchronous Motors

Tsuyoshi Nagano*, Student member, Goh Teck Chiang*, Member Jun-ichi Itoh*a), Member

(Manuscript received Jan. 00, 20XX, revised May 00, 20XX)

This paper proposes a parallel operation system of permanent magnet synchronous motors (PMSMs) and verifies the suppression effect of the proposed damping control for the torque vibration caused by resonance between synchronous reactance and inertia moment. The proposed system is composed by two types of power converters, a main inverter with a V/f control and an auxiliary inverter with the field-oriented control and the damping control. In general, PMSM cannot be driven by the V/f control such as an induction motor because the speed vibration is caused by the resonance between the synchronous reactance and the inertia moment. In the proposed system, the multiple PMSMs are driven in parallel by the main inverter with the V/f control. When the motor speed vibration occurs, the damping control for the auxiliary inverter suppresses this vibration in PMSM. From the frequency characteristics, it is clear that the power capacity of the auxiliary inverter is 10% lower than that of the main inverter when the frequency components included in the speed command are lower than 12 rad/s. As a result, the experimental results demonstrated that the proposed system can reduce the speed vibration from 400 r/min to nearly 0 r/min with the damping control in our prototype of 1500-W PMSM drive system. The experimental results well agree with the theoretical analysis results.

Keywords : Permanent magnet synchronous motor, Auxiliary inverter, Parallel drive

1. Introduction

Recently, the adjustable speed drive techniques for the permanent magnet synchronous motor (PMSM) have attracted a lot of attentions among the researchers in terms of the energy saving [(1)-(4)]. PMSM has high efficiency and high power density in comparison with the induction motor (IM) because PMSM does not have the excitation circuit. On the other hand, IMs can be driven in parallel by utilizing only one inverter. IM drive systems, in which multiple IMs are driven by one inverter, are applied to industry in terms of cost reduction and simplification of the system, because this system only utilizes one large power capacity inverter to drive multiple induction motors [(5)-(7)].

The efficiency of the motor drive system is improved by replacing IM with PMSM. However, it is difficult to drive the parallel connected PMSMs by using only one inverter because the torque vibration occurs due to the resonance between synchronous reactance and inertia moment of PMSM [(8)]. When the parallel connected PMSMs are driven by one inverter, the current cannot be controlled corresponding to each pole of PMSM because the pole position of the one PMSM is different from that of other PMSMs. Therefore, the torque vibration occurs unavoidably in this multiple PMSMs drive system.

The damping control that uses the current feedback has been proposed [(9)]. This method suppresses the torque vibration by adding the vibrational component in the effective current to the output phase command of the voltage command. However, this method cannot be applied to the parallel connected PMSMs because only one inverter cannot control each current corresponding to each pole of the PMSMs.

There are some literatures in which two PMSMs are driven by one power converter [(10)-(15)]. These converters can drive two PMSMs independently. However, these converters have some problems. For instance, the five-leg inverter [(10)-(12)] and the nine-switch inverter [(13)-(14)] are driven at low voltage utilization ratio in comparison with the case when one PMSM is driven by these converters because DC-link voltage is distributed to two PMSMs. Moreover, the current capacity of the switching device increases because there is one common leg. The four-leg inverter using the neutral point of the DC link capacitor utilizes fewer the switches than other topologies [(15)]. However, this converter requires the capacitor voltage balancing control because the capacitor neutral-point voltage is unbalanced by the motor current. Therefore, it is difficult to apply these converters to several PMSMs because the output voltage of the inverter is limited and the number of switching devices increases.

In this paper, in order to drive PMSMs in parallel effectively, a multi-parallel PMSMs drive system based on V/f control is proposed, and the proposed damping control is verified in the experiment. In the proposed method, the torque vibration is suppressed by an auxiliary inverter and auxiliary windings in each PMSM. The power capacity of the auxiliary inverter is much smaller than that of the main inverter because the output power of the auxiliary inverter is only used to suppress the vibration. Note that the proposed system assumes that the each PMSM in the multi-parallel connected PMSMs drives at same speed or

a) Correspondence to: Jun-ichi Itoh. E-mail: itoh@vos.nagaokaut.ac.jp
* Nagaoka University of Technology
1603-1, Kamitomioka-cho, Nagaoka, Niigata, Japan 940-2188

independent load such as industrial fans, pumps and flywheel energy storage systems. Different speed drive systems such as the electric train or electric vehicles are not considered in this paper because the motor speed of each PMSM is different from each other.

This paper is organized as follows; first, the configuration of the proposed parallel drive system is introduced. Next, the control method, which is comprised of V/f control for the main inverter and field-oriented control (FOC) for the auxiliary inverter, is described. Next, the stability of the proposed system is analyzed by the root locus. After that, the suppression effect of the damping control and the minimum power capacity of the auxiliary inverter are clarified from the frequency characteristics of the transfer function. Finally, the experimental results demonstrate that the proposed system drives the PMSM with suppressing the torque vibration and the experimental results agree with the theoretical analysis results.

2. Proposed Multiple PMSMs Drive System

2.1 System Configuration Fig. 1 shows the configuration of the proposed system. In PMSMs, the auxiliary windings which are used in the damping control (with the auxiliary inverter) are placed in the slots together with the main windings. The proposed system uses two different power rating inverters. The first one is the large power capacity inverter for the main windings to control the speed of the parallel connected PMSMs. The second one is the small power capacity inverter for the auxiliary windings to suppress the torque vibration. In terms of the effectiveness of the proposed system, it is very important that the power capacity of the auxiliary inverter is much smaller than that of the main inverter. In other words, the damping power for the PMSM is required much smaller than that of the main drive power. Moreover, the auxiliary inverter does not need to the external power supply depending on the operation condition because the DC link voltage of the auxiliary inverter is controlled using the active power. Therefore, when the capacitor can be only connected to DC link of the auxiliary inverter depending on the operation condition, the proposed system drives parallel connected PMSMs. The auxiliary inverters have little effect on the system cost because the power capacity of the auxiliary windings is enough smaller than the main windings.

2.2 Control Strategy Fig. 2 shows the control block diagram of the proposed system. In the proposed system, the V/f control is applied to the main inverter, and the FOC and the damping controls are applied to the auxiliary inverter. Each of the auxiliary inverter can control the current in auxiliary windings of the PMSM in order to suppress the torque and speed vibration. Since the torque and speed vibrations are caused by the phase difference between the rotational coordinates of the inverter and that of the PMSM, they can be suppressed by the damping control in the auxiliary inverter. Note that postion sensor-less vector control can be applied to auxiliary inverter when it is difficult to use position sensor.

Fig. 3 shows the relationship between the d-q rotating frame and the γ-δ rotating frame for V/f control. In the control of the auxiliary invereter, the direction of the flux vector with permanent magnet is defined as d-axis as same as the conventional FOC. In the V/f control, the output voltage vector is defined as δ-axis, the axis which lags by π/2 rad from δ-axis can be defined as γ-axis.

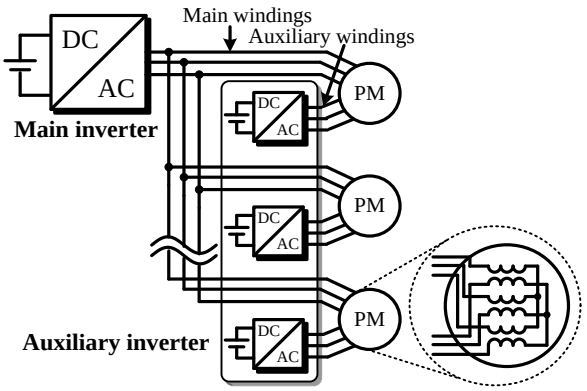

Fig. 1.Configuration of the proposed system that uses the large power capacity inverter for the motors and the small power capacity inverter for suppression of the vibration.

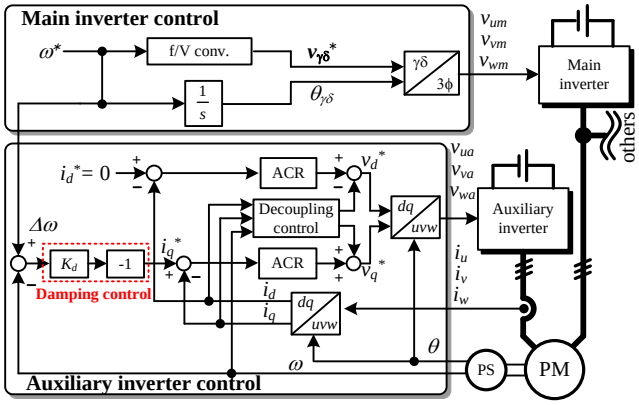

Fig. 2. Control block diagram of the proposed system. The V/f control is applied to the main inverter. The auxiliary inverters use the field-oriented control for the damping control.

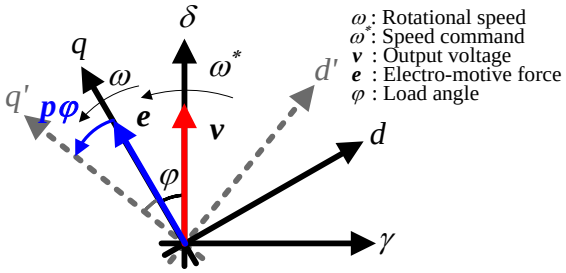

Fig. 3. Relationship between the d-q rotating frame and the γ-δ rotating frame. The γ-δ rotating frame lags by the load angle φ from the d-q rotating frame.

The lag of the load angle φ occurs between the d-q rotating frame and γ-δ rotating frame as shown in Fig. 3. Therefore, the load angle φ, rotational speed ω_{re} and the speed command ω^* can be expressed as

$$p\varphi = \omega_{re} - \omega^* \quad \text{.....(1)}$$

where p is differential operator.

When the vibration of the speed is caused by the resonance between the inertia moment and the synchronous reactance, the load angle φ also vibrates as shown (1). Then, the changes of the load angle $p\varphi$ is the difference between the rotational speed and

the speed command. In order to compensate the changes of the load angle $p\varphi$, the q-axis current command i_q* is calculated from the damping controller as shown in Fig. 2. As a result, the vibration of the speed and torque caused by the resonance are suppressed by compensating the changes of the load angle $p\varphi$ with the current controlled by the FOC and the damping control.

3. Stability Analysis

The damping control has to suppress the speed and torque vibration caused by the resonance between the inertia moment and the synchronous reactance in each PMSM. In the proposed system, the parallel connected PMSMs are driven while the resonance in each PMSM is suppressed. In this chapter, the stability of the proposed system with / without the damping control is clarified in the root locus. Note that this chapter analyzes the case that one PMSM is driven because the resonance occurs in each PMSM.

Fig. 4 shows the analysis model to confirm the suppression effect with the damping control. The proposed system uses the PMSM placed the auxiliary windings in the slots together with the main (conventional) windings, and so the mutual magnetic interference occurs between the main and the auxiliary windings. Due to the above reason, the control for the auxiliary inverter becomes complicated. Therefore, the proposed system is validated using a model where two PMSMs are connected in series via single shaft. Then, the rear end of the main PMSM is connected to the load machine. It means that the magnetic coupling is neglected in the analysis and the experiment.

The voltage equation of the motor that is connected to the main inverter is represented as the voltage equation in the γ-δ rotating frame because the main inverter is driven by the V/f control. Note that the γ-δ rotating frame lags by the load angle φ from the d-q rotating frame as shown in Fig. 3. On the other hand, the voltage equation of the motor that is connected to the auxiliary inverter is represented as the voltage equation in the d-q reference frame because the auxiliary inverter control is FOC. Therefore, the voltage equation of the motor that is connected to the main inverter in the estimated rotating γ-δ frame is given by

$$\begin{bmatrix} v_{M\gamma} \\ v_{M\delta} \end{bmatrix} = \begin{bmatrix} R_M + pL_{dM} & -\omega^* L_{qM} \\ \omega^* L_{dM} & R_M + pL_{qM} \end{bmatrix} \begin{bmatrix} i_{M\gamma} \\ i_{M\delta} \end{bmatrix} + \omega_{re}\psi_{mM} \begin{bmatrix} \sin\varphi \\ \cos\varphi \end{bmatrix} \quad \text{.....(2)}$$

On the other hand, the voltage equation of the motor that is connected to the auxiliary inverter in d-q reference frame can be given by

$$\begin{bmatrix} v_{Ad} \\ v_{Aq} \end{bmatrix} = \begin{bmatrix} R_A + pL_{dA} & -\omega_{re}L_{qA} \\ \omega_{re}L_{dA} & R_A + pL_{qA} \end{bmatrix} \begin{bmatrix} i_{Ad} \\ i_{Aq} \end{bmatrix} + \begin{bmatrix} 0 \\ \omega_{re}\psi_{mA} \end{bmatrix} \quad \text{.....(3)}$$

Moreover, torque and speed equation can be given by

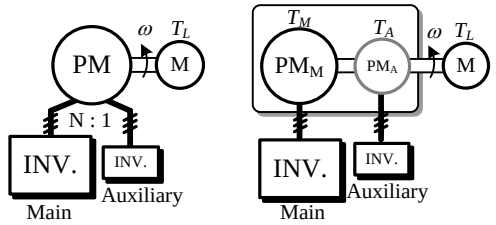

(a) Connection diagram (b) Simplification model

Fig. 4. Simulation model of the PMSM in addition auxiliary windings for damping control.

$$T = T_M - T_A = \frac{3}{2}P_{fM}\psi_{mM}\left(i_{M\gamma}\sin\varphi + i_{M\delta}\cos\varphi\right) - \frac{3}{2}P_{fA}\psi_{mA}i_{Aq} \quad \text{.....(4)}$$

$$p\omega_{re} = \frac{1}{J}\left(P_{fM}T_M - P_{fA}T_A\right) \quad \text{.....(5)}$$

where p is differential operator, R is armature resistance, L is synchronous reactance, P_f is the number of pole pairs of the pole, Ψ_m is magnet flux linkage, φ is the load angle, and J is the inertia moment of motors. Suffix 'A' represents the parameter of the motor that is connected to the auxiliary inverter, 'M' represents the parameter of the motor that is connected to the main inverter.

Equations (2) and (3), (4) are non-linear so that these equations are linearized around the steady state. The state equation after the linearization can be given by (6).

Equation (6) shows the 6th order of the state equation that is complicated to evaluate the stability. In order to simplify this equation, it is assumed that the mechanical time constant is larger than enough electrical time constant, then (6) can be approximated as the 2nd order state equation, as (7).

$$\begin{bmatrix} p\Delta\omega_{re} \\ p\Delta\varphi \end{bmatrix} = \begin{bmatrix} -\frac{3}{2}\frac{P_{fM}^2\psi_{mM}}{J} & \frac{\psi_{mM}R_M}{\omega_0^2 L_{dM}L_{qM}} & \frac{3}{2}\frac{P_{fM}^2\psi_{mM}^2}{JL_{qM}} \\ -1 & & 0 \end{bmatrix} \begin{bmatrix} \Delta\omega_{re} \\ \Delta\varphi \end{bmatrix}$$

$$+ \begin{bmatrix} \frac{3}{2}\frac{P_f^2\psi_{mM}R_M}{J\omega_0^2 L_{dM}L_{qM}} & -\frac{3}{2}\frac{P_f^2\psi_{mA}}{JR_A} & 0 \\ 0 & 0 & 1 \end{bmatrix} \begin{bmatrix} \Delta v_{M\delta} \\ \Delta v_{Aq} \\ \Delta\omega_1 \end{bmatrix} \quad \text{.....(7)}$$

where suffix '0' is the steady state value.

Above equation is the 2nd order state equation when the load angle is zero, the γ-axis current is zero and the δ-axis current is zero in the steady state. In addition, equation (7) assumes that the FOC is applied with the non-interference control and the γ-axis voltage command $\Delta v_{M\gamma}$* of the main inverter is zero as shown in Fig. 3. Note that the characteristic equation can be solved as ωL is larger than R from the state transition matrix **A** of (7). The damping factor ζ and the natural angular frequency ω_n, when the PMSM is

$$\begin{bmatrix} p\Delta i_{M\gamma} \\ p\Delta i_{M\delta} \\ p\Delta i_{Ad} \\ p\Delta i_{Aq} \\ p\Delta\omega_{re} \\ p\Delta\varphi \end{bmatrix} = \begin{bmatrix} -\frac{R_M}{L_M} & \omega_0 & 0 & 0 & -\frac{\psi_{mM}}{L_M}\sin\varphi_0 & -\frac{\omega_0\psi_{mM}}{L_M}\cos\varphi_0 \\ -\omega_0 & -\frac{R_M}{L_M} & 0 & 0 & -\frac{\psi_{mM}}{L_M}\cos\varphi_0 & \frac{\omega_0\psi_{mM}}{L_M}\sin\varphi_0 \\ 0 & 0 & -\frac{R}{L_A} & 0 & 0 & 0 \\ 0 & 0 & 0 & -\frac{R}{L_A} & 0 & 0 \\ \frac{3}{2}\frac{P_{fM}^2\psi_{mM}}{J}\sin\varphi_0 & \frac{3}{2}\frac{P_{fM}^2\psi_{mM}}{J}\cos\varphi_0 & 0 & -\frac{3}{2}\frac{P_{fA}^2\psi_{mA}}{J} & 0 & \frac{3}{2}\frac{P_{fM}^2\psi_{mM}}{J}\left(i_{M\gamma 0}\cos\varphi_0 - i_{M\delta 0}\sin\varphi_0\right) \\ 0 & 0 & 0 & 0 & -1 & 0 \end{bmatrix} \begin{bmatrix} \Delta i_{M\gamma} \\ \Delta i_{M\delta} \\ \Delta i_{Ad} \\ \Delta i_{Aq} \\ \Delta\omega_{re} \\ \Delta\varphi \end{bmatrix} + \begin{bmatrix} \frac{1}{L_M} & 0 & 0 & 0 & i_{M\delta 0} \\ 0 & \frac{1}{L_M} & 0 & 0 & -i_{M\gamma 0} \\ 0 & 0 & \frac{1}{L_A} & 0 & 0 \\ 0 & 0 & 0 & \frac{1}{L_A} & 0 \\ 0 & 0 & 0 & 0 & 0 \\ 0 & 0 & 0 & 0 & 1 \end{bmatrix} \begin{bmatrix} \Delta v_{M\gamma} \\ \Delta v_{M\delta} \\ \Delta v_{Ad} \\ \Delta v_{Aq} \\ \Delta\omega^* \end{bmatrix}$$

.....(6)

driven with only V/f control, can be given by

$$\zeta = 0 \quad \text{.....(8)}$$

$$\omega_n = \sqrt{\frac{3}{2}} \frac{P_{fM}\psi_{mM}}{\sqrt{JL_{qM}}} \quad \text{.....(9)}$$

As mentioned above, when the PMSM is driven with only V/f control, the resonance between the synchronous reactance and the inertia moment of the motor causes the torque vibration. On the other words, this vibration is unavoidable because the damping factor ζ is zero. Then, the 2nd order state equation to which the damping control is applied is derived.

Fig. 5 shows the state variable diagrams of the auxiliary inverter control that is applied with the damping control. In Fig. 5, the q-axis voltage command Δv_{Aq}*, it is assumed that the loop gain in the current control is 1 (assuming that the current control response is faster than the damping control response), can be given by

$$\Delta v_{Aq} = -K_d\left(\Delta\omega^* - \Delta\omega_{re}\right) \quad \text{.....(10)}$$

$$p\Delta x_1 = 0 \quad \text{.....(11)}$$

where K_d is the damping gain.

Moreover, in Fig. 3, the δ-axis voltage command $\Delta v_{M\delta}$* and the γ-axis voltage command $\Delta v_{M\gamma}$* of the main inverter are given by

$$\Delta v_{M\gamma} = 0 \quad \text{.....(12)}$$

$$\Delta v_{M\delta} = \psi_{mM}\Delta\omega^* \quad \text{.....(13)}$$

Substituting (10) and (13) into (7) yields the state equation of

$$p\mathbf{x} = \mathbf{A}\mathbf{x} + \mathbf{B}\mathbf{u} \quad \text{.....(14)}$$

where $\mathbf{x} = [\Delta\omega_{re} \quad \Delta\varphi]$, $\mathbf{u} = \Delta\omega^*$

$$\mathbf{A} = \begin{bmatrix} -\frac{3}{2}\frac{P_{fM}{}^2\psi_{mM}}{J}K_d & \frac{3}{2}\frac{P_{fM}{}^2\psi_{mM}{}^2}{JL_{qM}} \\ -1 & 0 \end{bmatrix}, \mathbf{B} = \begin{bmatrix} \frac{3}{2}\frac{P_{fM}{}^2\psi_{mM}}{J}K_d \\ 1 \end{bmatrix}$$

Fig. 6 shows the transition of the pole placement (the root locus) with the damping control when the damping gain K_d is gradually changed. The poles when the proposed system is applied without/with the damping control are given by

$$s = \pm i\sqrt{\frac{3}{2}} \frac{P_{fM}\psi_{mM}}{\sqrt{JL_{qM}}} \quad \text{.....(15)}$$

$$s = -\frac{3}{2}\frac{P_{fM}{}^2\psi_{mM}}{2J}K_d \pm i\sqrt{\frac{3}{2}}\frac{P_{fM}\psi_{mM}}{\sqrt{JL_{qM}}}\sqrt{\left(\sqrt{\frac{3}{2}}P_{fM}\frac{K_d}{2}\sqrt{\frac{L_{qM}}{J}}\right)^2 - 1} \quad \text{...(16)}$$

At the damping gain $K_d = 0$, the poles are placed on the imaginary axis as shown in (15). In other words, when the damping control is not applied, it shows that the proposed system is unstable. By contrast, when the damping gain K_d increases, the poles move into left half plane as shown in (16). Therefore, PMSM can be driven stably in the proposed system by applying the damping control.

4. Theoretical Analysis of Suppression Characteristics

4.1 Suppression Effect of Damping Control The damping control has to suppress the speed and torque vibration caused by the resonance between the inertia moment and the synchronous reactance. This resonance is caused by the drastic change of the speed command. In this chapter, the suppression effect of the damping control is clarified from the frequency characteristics from the speed command to rotational speed in the proposed system.

The transfer function is derived from the 2nd state equation of (14). The speed command $\Delta\omega$* to the rotational speed $\Delta\omega_{re}$ transfer function is given by

$$\frac{\Delta\omega_{re}}{\Delta\omega^*} = \frac{\frac{3}{2}\frac{P_f{}^2\psi_{mM}}{J}}{s^2 + \frac{3}{2}\frac{P_f{}^2\psi_{mM}}{J}K_d s + \frac{3}{2}\frac{P_f{}^2\psi_{mM}{}^2}{JL_{qM}}} \times \left\{\frac{\psi_{mM}}{L_{qM}} - s\left(K_d + \frac{\left(i_{M\gamma 0}\cos\varphi_0 + i_{M\delta 0}\sin\varphi_0\right)}{\omega_0} - \frac{\psi_{mM}}{L_{qM}\omega_0}\sin\varphi_0\right)\right\} \quad (17)$$

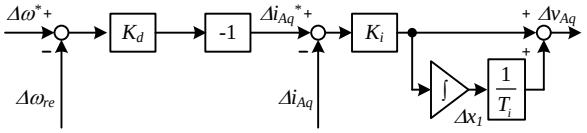

Fig. 5. State variable diagrams of the auxiliary inverter control. If the current control response is faster than the damping control response, the loop gain in the current control is 1. Therefore, the q-axis voltage command Δv_{Aq}* can be given by (10).

Table 1. Analysis and experimental conditions

	PM_M	PM_A
Rated power [W]	1500	750
Rated speed [min^{-1}]	1800	
Rated current [A]	8.2	4
Number of pole pairs	3	3
Armature resistance [Ω]	1.55	1.98
d-axis inductance [mH]	11.5	15.2
q-axis inductance [mH]	23	33.2
Electro-motive force constant [Vs/rad]	0.368	0.338
Inertia moment [kgm^2]	0.0051	0.0026
Rotational speed in stationary state [rad/s]	900	

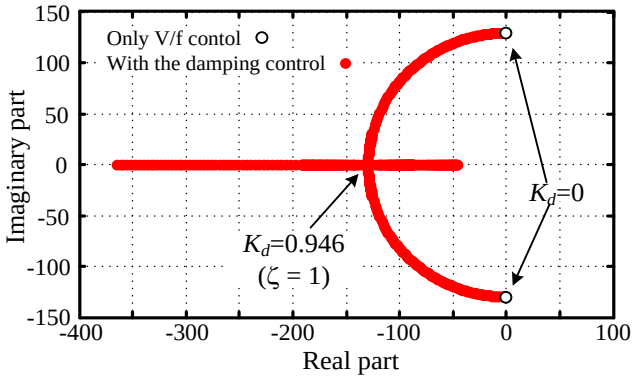

Fig. 6. Root locus with the control structures in the proposed system. Table I shows the evaluated condition. When the damping control is not applying, it shows that the proposed system is unstable. By contrast, when the damping gain K_d increases, the poles move into left half plane.

The damping factor ζ and the natural angular frequency ω_n are given by

$$\zeta = \sqrt{\frac{3}{2}} \frac{P_{fM} K_d}{2} \sqrt{\frac{L_{qM}}{J}} \quad \text{.....(18)}$$

$$\omega_n = \sqrt{\frac{3}{2}} \frac{P_{fM} \psi_{mM}}{\sqrt{JL_{qM}}} \quad \text{.....(19)}$$

4.2 Minimum Power Capacity of Auxiliary Inverter In the previous section, it is confirmed that the resonance between the synchronous reactance and the inertia moment is suppressed by the damping control in the proposed system. However, in order to obtain the larger suppression effect, the damping gain K_d has to be increased, the output power of the auxiliary inverter becomes larger. Moreover, the power capacity of the auxiliary inverter depends on the speed command response. Thus, in this section, the minimum power capacity of the auxiliary inverter is clarified from frequency characteristics using the transfer function from the output power command, which is calculated by the speed command, to the output power of the auxiliary inverter. In the proposed system, the main torque cannot be controlled directly due to the V/f control. However, with calculating the transfer function from the output power command to the output power, the frequency characteristic of each output power is derived. If the electrical and mechanical losses are neglected, the output power of the auxiliary inverter depends on the mechanical output of the motor. In other words, the transfer function of the output power for the auxiliary inverter is derived from the mechanical output transfer function of the motor. However, the mechanical output is nonlinear because the mechanical output is the product of two variables; the rotational speed and the torque. Due to this reason, the transfer function of the output power of the auxiliary inverter is derived after the mechanical output is linearized. Then, the transfer function from the speed command to the output power of the auxiliary inverter is given by

$$\frac{\Delta P_A}{\Delta \omega^*} = \frac{s^2 \frac{3}{2} \omega_0 K_d \psi_{mA}}{s^2 + \frac{3}{2} \frac{P_{fM}{}^2 \psi_{mM}}{J} K_d s + \frac{3}{2} \frac{P_{fM}{}^2 \psi_{mM}{}^2}{JL_{qM}}} \quad \text{.....(20)}$$

Moreover, the transfer function from the power which is caused by the speed command to the output power of the auxiliary inverter, it is assumed as $\delta_0 = 0$, $i_{M\gamma 0} = 0$, $i_{M\delta 0} = 0$ in (20), is given by

$$\frac{\Delta P_A}{\Delta P^*} = \frac{s \frac{3}{2} \frac{K_d \psi_{mA}}{J}}{s^2 + \frac{3}{2} \frac{P_{fM}{}^2 \psi_{mM}}{J} K_d s + \frac{3}{2} \frac{P_{fM}{}^2 \psi_{mM}{}^2}{JL_{qM}}} \quad \text{.....(21)}$$

where the relationship between the speed command and the power P^* which is caused by the speed command is given by

$$\frac{\Delta \omega^*}{\Delta P^*} = \frac{1}{J \omega_0 s} \quad \text{.....(22)}$$

4.3 Relation between Acceleration in Speed Command and Output Power of Auxiliary Inverter In section 4.2, the output power of the auxiliary inverter was discussed by frequency characteristics. However, the acceleration or deceleration time is set as the speed command in practically. In this session, the output power of the auxiliary inverter is discussed by acceleration which means the rate of the speed command.

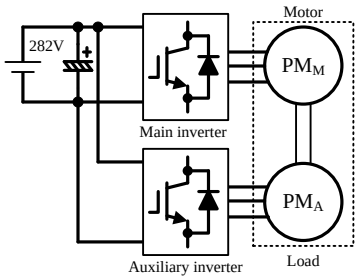

Fig. 7. Experimental construction in order to verify the suppress effect of damping control

The time response of the rotational speed is derived from the inverse Laplace transform of the ramp response of (17). In this section, in order to simplify (17), it is assumed as $\varphi_0 = 0$, $i_{M\gamma 0} = 0$ and $i_{M\delta 0} = 0$ in (17). Moreover, the overshoot of the rotational speed can be derived from this time response, as given by

$$\Delta \omega_{re\_Overshoot} = \frac{\alpha \sin\left(\omega_n t_{peak} \sqrt{1-\zeta^2}\right)}{\omega_n \sqrt{1-\zeta^2} \exp\left(\zeta \omega_n t_{peak}\right)} \quad \text{..... (23)}$$

$$t_{peak} = \frac{1}{2} \frac{\log\left(2\zeta^2 - 1 + 2\zeta\sqrt{\zeta^2 - 1}\right)}{\omega_n \sqrt{\zeta^2 - 1}} \quad \text{..... (24)}$$

where α [rad/s^2] is acceleration.
The overshoot of the rotational speed can be calculated by using (23).

Similarly, the time response of the output power of the auxiliary inverter during the acceleration is also derived from the inverse Laplace transform of the ramp response of (20). In this section, in order to simplify (20), it is assumed as $\delta_0 = 0$, $i_{M\gamma 0} = 0$, $i_{M\delta 0} = 0$ in (20). Moreover, the maximum output power of the auxiliary inverter can be derived from this time response, as given by

$$\Delta P_{aPeak} = \frac{\frac{3}{2} P_f \psi_{mA} K_d \omega_0 \alpha \sin\left(\omega_n \sqrt{1-\zeta^2} t_{peak}\right)}{\omega_n \sqrt{1-\zeta^2} \exp\left(\zeta \omega_n t_{peak}\right)} \quad \text{..... (25)}$$

The maximum output power of the auxiliary inverter can be calculated by (25).

5. Experimental Verifications

5.1 Experimental Set-up In this chapter, in order to confirm the effectiveness of the damping control, the experiments are demonstrated with a motor - generator set.

Fig. 7 shows the experimental configuration to confirm the effectiveness of the damping control in the proposed system. The proposed system uses the PMSM placed the auxiliary windings in the slots together with the main (conventional) windings, and so the mutual magnetic interference occurs between the main and the auxiliary windings. Due to the above reason, the control for the auxiliary inverter becomes complicated. Therefore, in order to verify the proposed system, the proposed system is validated using a model where two PMSMs are connected in series via single shaft such as the motor-generator (M-G) set in the experiment. Note that the motor and generator work as main windings and the auxiliary windings, respectively. As mentioned above, the effectiveness of the proposed system can be also verified with the M-G set as shown in Fig. 7.

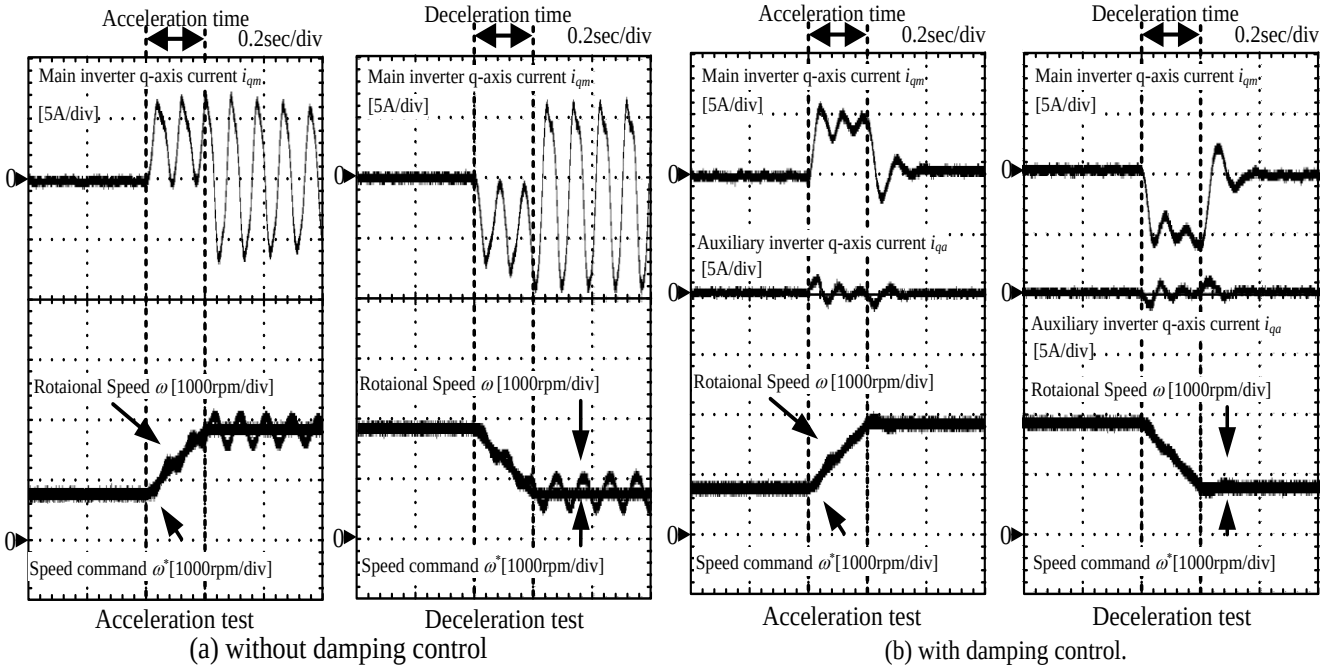

Fig. 8. Acceleration and deceleration test without/with damping control in motor-generator set. (a) After the acceleration, the 400 r/min - speed vibration is maintained. (b) The speed vibration is reduced from 400 r/min to nearly 0 r/min in compared with (a)

5.2 Damping Control Fig. 8 shows the experimental results that illustrate the motor speed vibration when the proposed system is applied (a) without the damping control and (b) with the damping control ($\zeta = 0.3$) in an acceleration and deceleration test. In this experiment, it is difficult to measure the torque response directly. Therefore, the speed vibration is evaluated instead of the torque response. In Fig. 8(a), the proposed system is implemented without the damping control. The speed vibration occurs during the acceleration. After the acceleration, a 400 r/min of speed vibration and the 10 $A_{p\text{-}p}$ of current vibration in q-axis of the main inverter are maintained. On the other hand, Fig. 8(b) demonstrates the experimental results, where the proposed system is implemented with the damping control ($\zeta = 0.3$). The effectiveness of the auxiliary inverter from the results confirms that the speed vibration is reduced from 400 r/min to nearly 0 r/min in compared with the acceleration test of Fig. 8(a). The 10 $A_{p\text{-}p}$ of the current vibration in the q-axis of the main inverter is suppressed as well. Then, the output power of the auxiliary inverter is suppressed to 13% of the main inverter when the damping factor is designed at 0.3. In the same way as the acceleration test of Fig. 8(a), after the deceleration, a 500 r/min of speed vibration and the 15 $A_{p\text{-}p}$ of current vibration in q-axis of the main inverter are maintained as shown in the deceleration test of Fig. 8(a). In contrast, it is confirmed that, as shown the deceleration test of Fig. 8(b), the speed vibration is reduced from 500 r/min to nearly 0 r/min and the current vibration is reduced from 15 $A_{p\text{-}p}$ to 0 $A_{p\text{-}p}$ in compared to Fig. 8(a) in the same way as acceleration test. Nevertheless, it is confirmed that the q-axis current of the auxiliary inverter flows only during acceleration and deceleration. Moreover, the maximum q-axis current of the auxiliary inverter is 20% of the q-axis current of the main inverter. Therefore, it is confirmed that the auxiliary inverter can suppress the speed vibration via auxiliary windings with a small q-axis current of the auxiliary inverter even if in the acceleration and deceleration test.

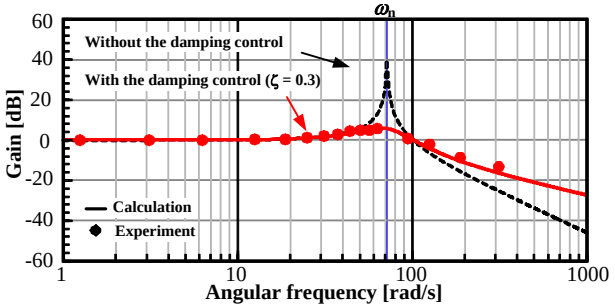

Fig. 9. Frequency characteristics of the speed command to the rotational speed in the proposed system. Table I shows the evaluated condition. By applying the damping control, the magnitude at the resonance frequency decreases to 5 dB.

5.3 Frequency Characteristics of Proposed Damping Control The frequency characteristics are demonstrated by the experimental results in order to confirm the validity of the theoretical analysis. Moreover, the suppression effect of the damping control is discussed by comparing the peaks of the amplitude on the resonance frequency band.

Fig. 9 shows the frequency characteristic of the transfer function (17) from the speed command to rotational speed of the V/f control. Table 1 shows the analysis and experimental conditions. In Fig. 9, the magnitude at the resonance frequency ω_n becomes lower with the damping control in comparison to the proposed system without the damping control. It means that the suppression effect becomes higher with the proposed damping control. Without the damping control ($\zeta = 0$), the magnitude at the resonance frequency rises. By contrast, with the damping control ($\zeta = 0.3$), the magnitude at the resonance frequency decreases to 5 dB. The high suppression effect is obtained by increasing the damping gain as shown (18) because the damping factor increases. Therefore, the suppression effect of the damping control is

clarified from the frequency characteristics of the transfer function (17) from the speed command to rotational speed in the proposed system. The proposed damping control can suppress the resonance between the moment inertia and synchronous reactance as show in Fig. 9. In the experiment, when the constant speed command adds sinusoidal wave as the speed command, the amplitude in the frequency of the sinusoidal wave is drawn by observing the speed response. The gain between the speed commands and rotational speed in the experimental results has been plotted in Fig. 9 as dot marks. The experimental results well agree with the analysis results.

5.4 Minimum Power Capacity of Auxiliary Inverter The power capacity of the auxiliary inverter depends on the transient response for the speed command as described in section 4.2. In order to confirm the theoretical analysis, the frequency characteristics between each output power and speed variation is investigated in the experiment.

Fig. 10 shows the frequency characteristics of the transfer function from the power command to the output power of the main inverter, the auxiliary inverter, and the sum of the inverters in the proposed system. In Fig. 10, the output power of the auxiliary inverter rises near the resonance frequency. On the other hand, when the frequency components into the speed command are lower and lower, the output power of the auxiliary inverter is suppressed more. In other words, the auxiliary inverter does not contribute steady state i.e. constant speed. Nevertheless, although the output power of the main inverter is constant because the main inverter drives the motor. Note that the damping factor is designed by (18). When the frequency components included in the speed command are lower than 12 rad/s, the output power of the auxiliary inverter can become lower than 10% of the main inverter as shown in Fig. 10. This boundary condition is decided by inertia moment J, q-axis inductance L_{qM}, magnet flux linkage Ψ_m and the damping gain K_d as shown in (21). When the damping gain K_d increases, the output power of the auxiliary inverter increase from 10% of the main inverter at 12 rad/s because the damping factor increases. Therefore, the results show that the power capacity of the auxiliary inverter can be designed to nearly several percent of the main inverter when the proposed system is applied to the application which requires slow speed response such as fan applications.

Fig. 11 shows the experimental waveforms that each output power is measured at each operating point in Fig. 10 when 0.5 p.u. of the constant speed command adds sinusoidal wave as the speed command. Assuming that the inverter output voltage is equal to the voltage command, each output power is calculated from the voltage command and the measured current. The waveforms in Fig. 11(a), (b) and (c) mention the operation at the point (a), (b) and (c) in Fig. 8, respectively. The other experimental results have been plotted in Fig. 10 as dot marks. Comparing with each result, the amplitude ratio between the output power of the auxiliary inverter and the main inverter is changed corresponding to the frequency components included in the speed command. The experimental results also well agree with the analysis results.

5.5 Relation between Acceleration in Speed Command and Output Power of Auxiliary Inverter In this session, in order to confirm the validity of proposed system in terms of acceleration which means the rate of the speed command, the relationship between the output power of the auxiliary inverter and

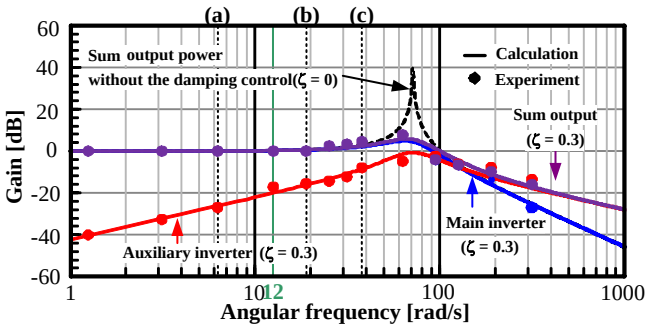

Fig. 10. Frequency characteristics of the transfer function from power command to output power of the main inverter, the auxiliary inverter, and the sum of the inverters in the proposed system.

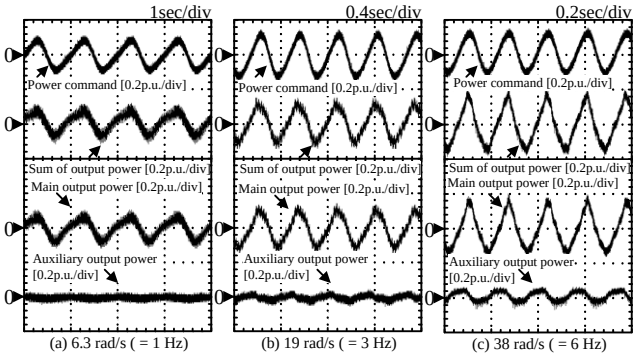

Fig. 11. Experimental results that each output power is measured at each operating point ((a) is at 1 Hz, (b) is at 3 Hz, (c) is 6 Hz) in Fig. 8 when 0.5 p.u. of the constant speed command adds sinusoidal wave as the speed command.

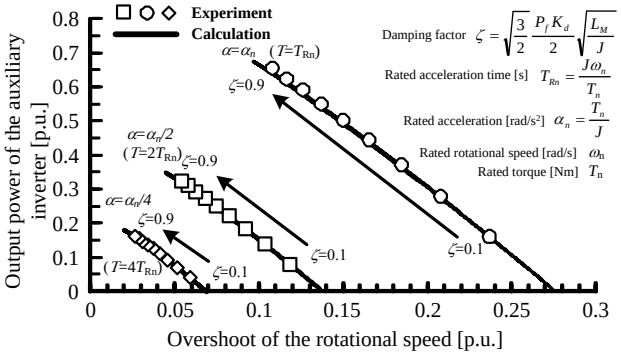

Fig. 12. Relationship between the output power of the auxiliary inverter and the overshoot of the rotational speed the against speed command. Table 1 shows also the evaluated condition. The higher suppression effect is obtained in exchange for the increase of the output power of the auxiliary inverter because of increasing the damping gain.

the overshoot of the rotational speed for speed command is demonstrated in the experiment.

Fig. 12 shows the relationship among the damping gain K_d, the maximum output power of the auxiliary inverter during the acceleration and the overshoot of the rotational speed when the PMSM is accelerated during one, half, quarter of the rated acceleration α_n on the condition as shown in Table 1. The damping gain is standardized by the damping factor ζ as given by (18). The output power of the auxiliary inverter rises with the increase of the

damping factor. On the other hand, the overshoot of the rotational speed decreases with the increase of the damping factor, as shown in Fig. 12. The maximum output power of the auxiliary inverter (i.e. the power capacity of the auxiliary inverter) depends on the acceleration factor α in the speed command as shown in Fig. 12. The experimental results well agree with the calculation.

6. Parallel Operation

Fig. 13 shows the simulation models that are used to verify the operation of two sets of parallel connected PMSM. Since it is difficult to construct our prototype of the drive system using two PMSMs, the simulation is used to evaluate the validity of the proposed controller as first step.

Fig. 14 shows the simulation results when two sets of parallel connected PMSMs are driven by the proposed system with the damping control. Smooth acceleration progresses are confirmed in the two set of parallel connected PMSMs. Besides, when the rated motor speed, load step applies to PMSM1 at 0.38s, and later also applies to PMSM2 at 0.42s, the operation of the two auxiliary inverters can be observed from the output power. The maximum output power of the auxiliary inverter is approximately 0.25 p.u. of the rated power of the main inverter. Although the power capacity of main inverter increases with the increase of parallel units, the power capacity of auxiliary inverter does not change according to the numbers of parallel units.

7. Conclusion

This paper proposes a control technique to drive multiple numbers of parallel connected PMSMs, and the proposed damping control by using the small auxiliary inverter and the auxiliary windings is analyzed theoretically and verified in the experiment. The stability of the proposed system is analyzed and discussed by the root locus. Moreover, the suppression effect of the damping control and the minimum power capacity of the auxiliary inverter were clarified from the frequency characteristics from the speed command to rotational speed in the proposed system.

In order to confirm the validity of the theoretical analysis, the experiments were demonstrated with a motor - generator set. The experimental results of the proposed system using 1.5 kW PMSM drive system are obtained as follows;

i) The proposed system with damping control can reduce the speed vibration from 400 r/min to nearly 0 r/min in spite of small q-axis current by suppressing the torque vibration.

ii) PMSM can be stabilized by the damping control.

iii) The output power of the auxiliary inverter is suppressed to 10% of the main inverter when the speed response is lower than 12 rad/s.

The experimental results well agree with the theoretical analysis results. Thus, the validity of the proposed system is confirmed by both the theoretical analysis and the experimental results.

In the future, PMSM added the auxiliary windings will be designed and made. Next, the decoupling control of PMSM added the auxiliary windings will be considered. In addition, driving two PMSMs added the auxiliary windings in parallel with the proposed system will be considered and evaluated. After that, the proposed system will be evaluated and analyzed in detail; for example, the necessity of external power supply connected the auxiliary inverter will be considered in the future.

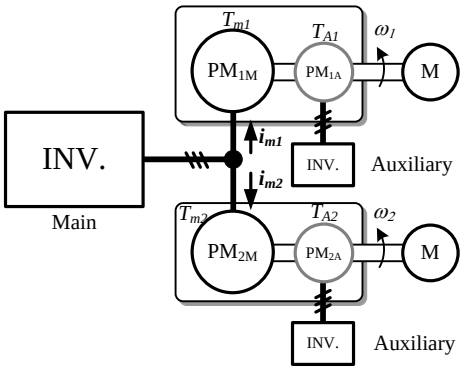

Fig. 13. Simulation model for parallel connected dual motor drive. In order to neglect the magnetic coupling, two parallel drive of the proposed system is validated using Fig. 8.

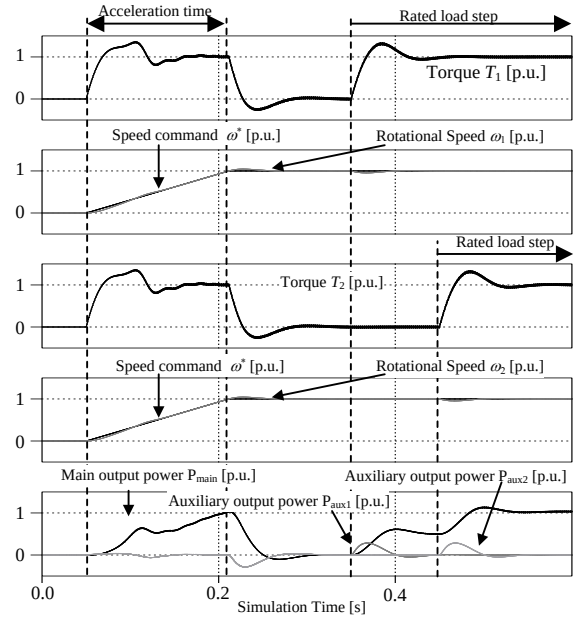

Fig. 14. Simulation results for parallel motor drive with damping control. Smooth acceleration progresses are confirmed in the two parallel connected PMSMs. After the rated motor speed, load step applies to each PMSM, stable operation of each PMSM can be confirmed.

A part of this study was supported by Industrial Technology Grant Program in 2011 from New Energy and Industrial Technology Development Organization (NEDO) of Japan.

References

(1) M. J. Corley, and R. D. Lorenz, "Rotor Position and Velocity Estimation for a Salient-Pole Permanent Magnet Synchronous Machine at Standstill and High Speeds", IEEE Trans. Industry Applications, Vol. 34, No. 4, pp. 784-789 (1998)

(2) Chan-Hee Choi, Jul-Ki Seok, and Lorenz, R.D. : "Wide-Speed Direct Torque and Flux Control for Interior PM Synchronous Motors Operating at Voltage and Current Limits", IEEE Trans. Industry Applications, Vol. 49, No.1, pp.119-117 (2013)

(3) Rahman, M.F., Zhong, L.,Khiang Wee Lim : "A direct torque-controlled interior permanent magnet synchronous motor drive incorporating field weakening", IEEE Trans. Industry Applications, Vol.34, No.6, pp.1246-1253 (1998)

(4) M. Nasir Uddin, Tawfik S. Radwan, and M. Azizur Rahman,: "Performance of interior permanent magnet motor drive over wide speed range", IEEE Trans. Energy Conversion, Vol.17, No.1, pp.79-84 (2002)

(5) Matsuse, K. ; Kouno, Y. ; Kawai, H. ; Yokomizo, S.: "A speed-sensorless vector control method of parallel-connected dual induction motor fed by a single inverter", IEEE Trans. Industry Applications., Vol.38, pp.1566-1571 (2002)
(6) J. D. Ma, B. Wu, N. R. Zargari, Steven C. Rizzo, "A Space Vector Modulated CSI-Based AC Drive for Multimotor Applications", IEEE Trans. POWER ELECTRONICS, VOL.16, NO.4, pp.535-544 (2001)
(7) A. Bouscayrol, M. Pietrzak-David, P. Delarue, R. Peña-Eguiluz, P. V. Kestelyn, "Weighted Control of Traction Drives With Parallel-Connected AC Machines", IEEE Trans. Industrial Electronics, Vol.53, No.6, pp.1799-1806 (2006)
(8) Al Jowder, F.A.R. , Boon-Teck Ooi "Series Compensation of Radial Power System by a Combination of SSSC and Dielectric Capacitors", IEEE Trans. Power Delivery, Vol. 20, No.1, pp.458-465 (2005)
(9) J, Itoh, N, Nomura, H, Ohsawa: "A Comparison between V/f Control and Position-Sensorless Vector Control for the Permanent Magnet Synchronous Motor", Proc. of the Power Conversion Conference PCC Osaka 2002, Vol. 3, pp.1310 - 1315 (2002)
(10) D. Dujic, M. Jones, S. N. Vukosavic, E. Levi, "A General PWM Method for a (2n + 1)-Leg Inverter Supplying n Three-Phase Machines", IEEE IEEE Trans. Industrial Electronics, Vol. 56, No. 10, pp.4107-4118 (2009)
(11) Ibrahim, Z.; Lazi, J.M. ; Sulaiman, M. : "Independent speed sensorless control of dual parallel PMSM based on Five-Leg Inverter", Proc. of the 9th International Multi-Conference on Systems, Signals and Devices, pp.1-6 (2012)
(12) L. Tang, G. J. Su, "High-Performance Control of Two Three-Phase Permanent-Magnet Synchronous Machines in an Integrated Drive for Automotive Applications", IEEE Trans. Power Electronics, Vol. 23, No. 6, pp.3047-3055 (2008)
(13) Seyed Mohammad, et al.: "Space Vectors Modulation for Nine-Switch Converters", IEEE Trans. Power Electronics, Vol.25, No. 6, pp.1488-1496 (2010)
(14) F. Gao, L. Zhang, D. Li, P. C. Loh, Y. Tang, H. Gao, "Optimal Pulsewidth Modulation of Nine-Switch Converter", IEEE Trans. Power Electronics, Vol. 25, No. 9, pp.2331-2342 (2010)
(15) Mori, T., Tanaka, H., Kubo, Y., Matsuse, K., "Independent vector control of two permanent magnet synchronous motors fed by a four-leg inverter", Proc. of the 2012 IEEE International Conference on Power Electronics, Drives and Energy Systems (PEDES), pp.1-6 (2012)

Tsuyoshi Nagano

(Student member) received his B.S. and M.S. degrees in electrical, electronics and information engineering from Nagaoka University of Technology, Niigata, Japan in 2012 and 2014, respectively. Since 2014, he has been with Nagaoka University of Technology as a Ph.D. degree student His research interests include motor drives. He is a student member of the Institute of Electrical Engineers of Japan.

Goh Teck Chiang

(Member) received his B.S. degree in electrical and electronic engineering from Queensland University of Technology, Brisbane, Australia in 2004. Then, he received his M.S. and Ph.D. degrees in electrical and electronic systems engineering from Nagaoka University of Technology, Niigata, Japan in 2009 and 2012, respectively. His research interests include indirect matrix converters, PWM and motor drive. He is a member of the Institute of Electrical Engineers of Japan.

Jun-ichi Itoh

(Member) received his M.S. and Ph.D. degrees in electrical and electronic systems engineering from Nagaoka University of Technology, Niigata, Japan in 1996 and 2000, respectively. From 1996 to 2004, he was with Fuji Electric Corporate Research and Development Ltd., Tokyo, Japan. Since 2004, He has been with Nagaoka University of Technology as an associate professor. He received the IEEJ Academic Promotion Award (IEEJ Technical Development Award) in 2007 and the Isao Takahashi Power Electronics Award in 2010. His research interests include matrix converters, DC/DC converters, power factor correction techniques and motor drives. He is a member of the Institute of Electrical Engineers of Japan.